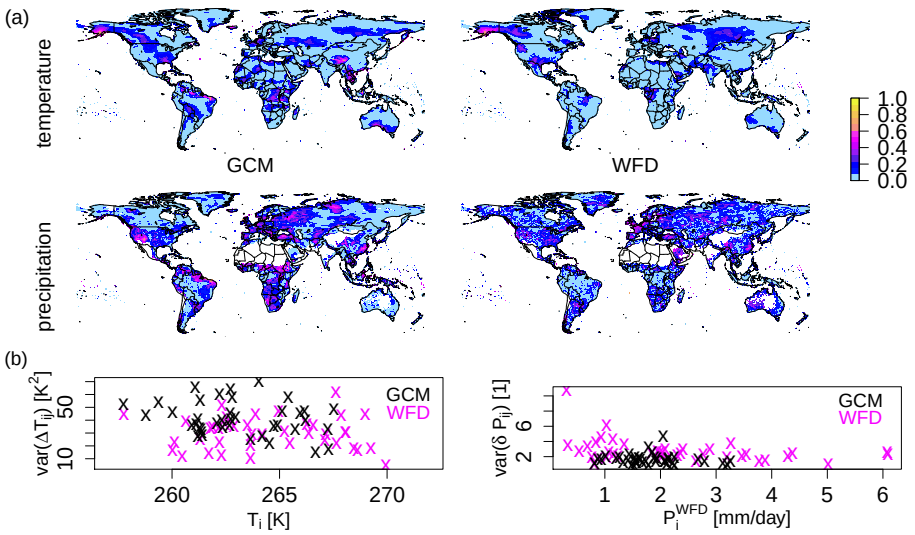

Figure S1: Linear dependence of the variances of anomalies on the monthly mean values. The residual temperature and normalised precipitation values for each April in the reference period are calculated and the related variances are estimated. These variances of the anomalies are analysed in dependence of the corresponding monthly mean values. (a) The coefficient of determination (R-squared) between variance and mean is estimated at each grid box to provide a global view on the dependence. Blue indicates low R-squared values which refer to marginal linear dependence, while yellow would indicate strong dependence. Dry regions where no correction of the variance of precipitation is performed are masked in the related map. (b) In the right panels scatter plots for the example grid box are shown from which the R-squared estimates for these coordinates originate.

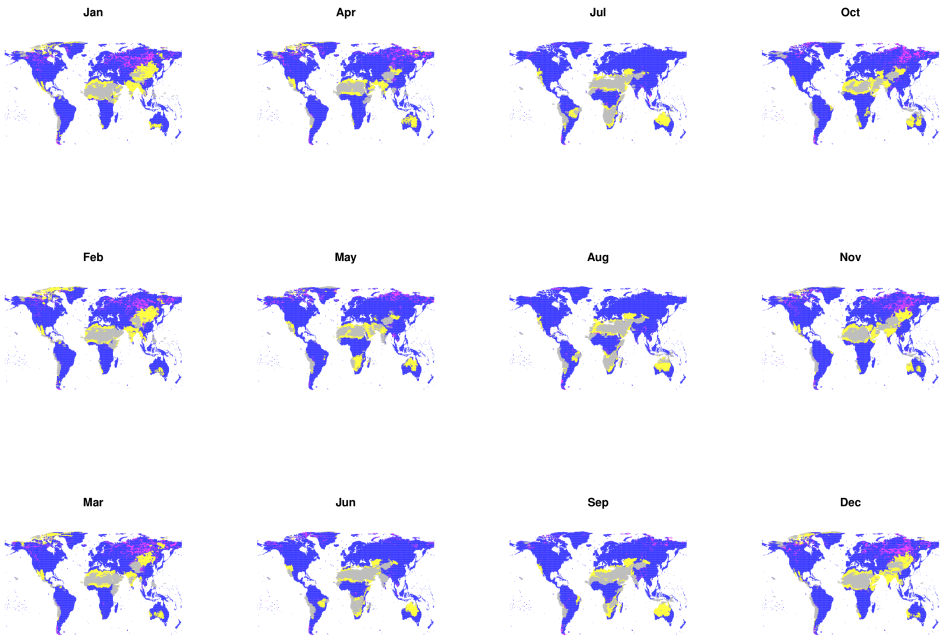

Figure S2: Illustration of the selected bias correction type, a correction of the monthly mean is applied in all cases. We distinguish three cases: Correction of daily data with a nonlinear transfer function (blue), with a linear transfer function (magenta) and no correction of daily data (yellow). In the latter case, grey areas additionally indicate regions there the monthly correction factor was truncated.

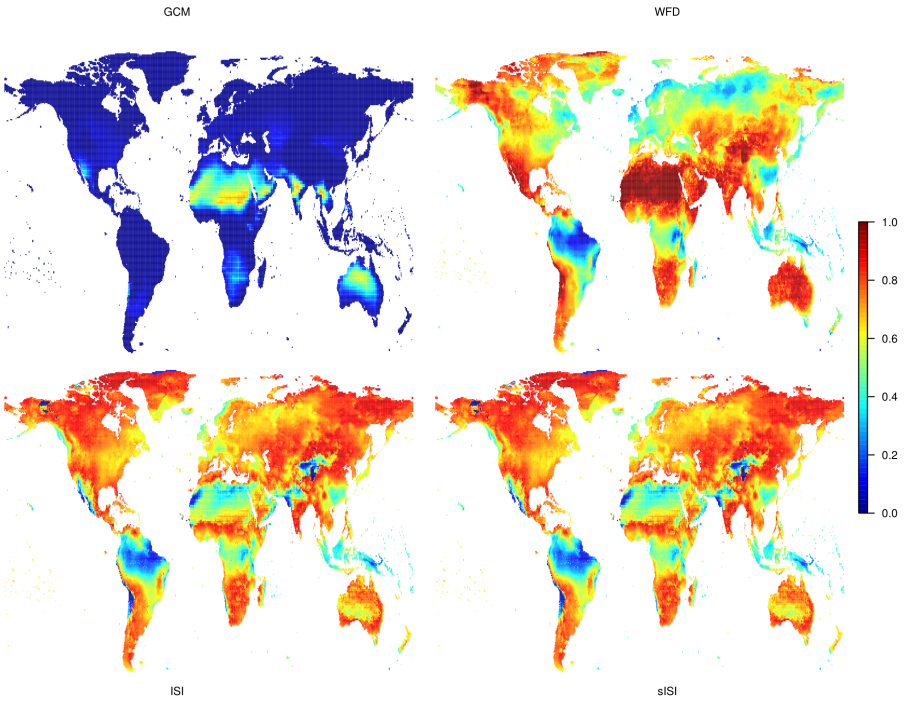

Figure S3: Portion of dry days in April over the period 1980 to 1999 – zero corresponds no dry days, one corresponds to all (i.e., 600) days dry. Uncorrected simulations (GCM) and observational data (WFD) are compared to bias-corrected simulation data relying on the reference 1960 to 1999 (ISI) or 1960 to 1979 (sISI).

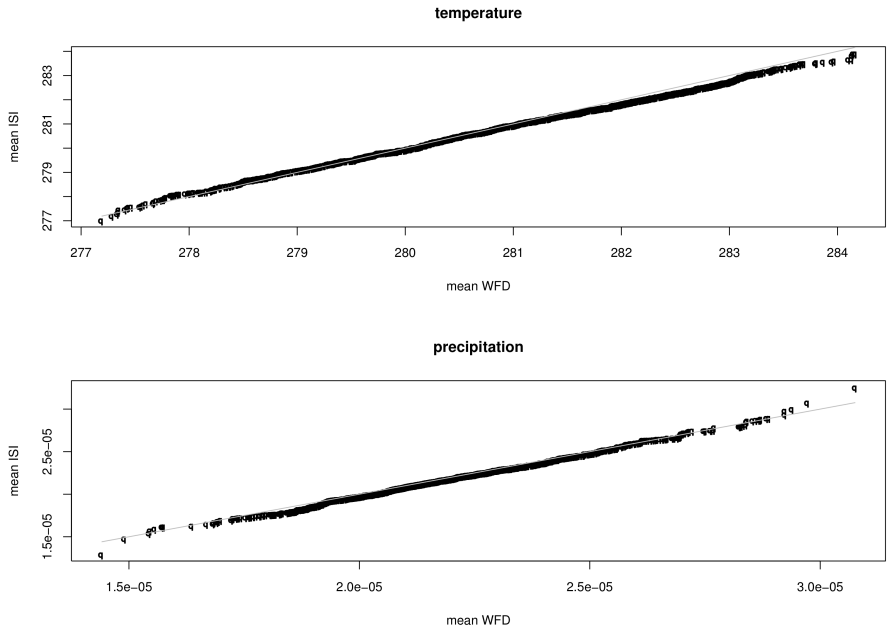

Figure S4: Quantile-quantile plot of land-averaged April temperature and precipitation values. Global average values obtained from the extended ISI-MIP bias correction method are ordered by ranks and plotted against rank-ordered global average values of WFD.

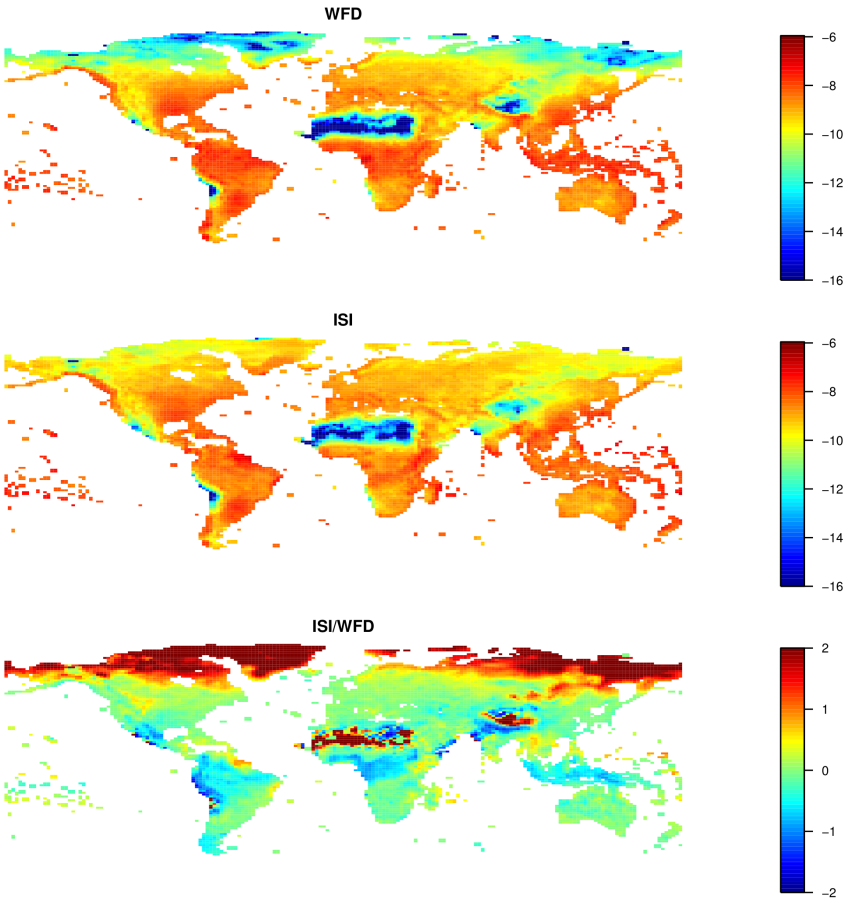

Figure S5: Illustration of the variances of the observed (WFD) and bias-corrected (ISI) April precipitation and the ratio of both. Decadic logarithms are shown. In case of the ratio, deviations that are larger than two orders of magnitude are obtained in some parts of the Sahara or in the high latitutes, but are not shown (i.e., 2 actually refers to 2 to 7.3). The variances are calculated for the reference period 1960 to 1999 from the daily precipitation (in mm s^{-1}) at the HadGEM2-ES resolution. The precipitation values where aggregated with a conservative remapping algorithm (using the Spherical Coordinate Remapping and Interpolation Package) to the model resolution.

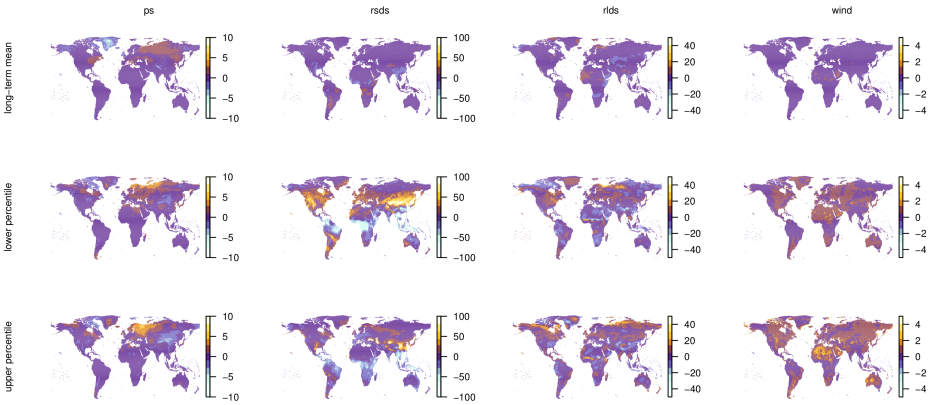

Figure S6: Differences between observations and the bias-corrected surface pressure (ps in hPa), short wave downward radiation (rsds in W m^{-2}), long wave downward radiation (rlds in W m^{-2}) and wind speed (wind in m s^{-1}) in terms of the long-term mean and the lower and upper interpercentile ranges. Results are shown for the ISI-MIP data set.

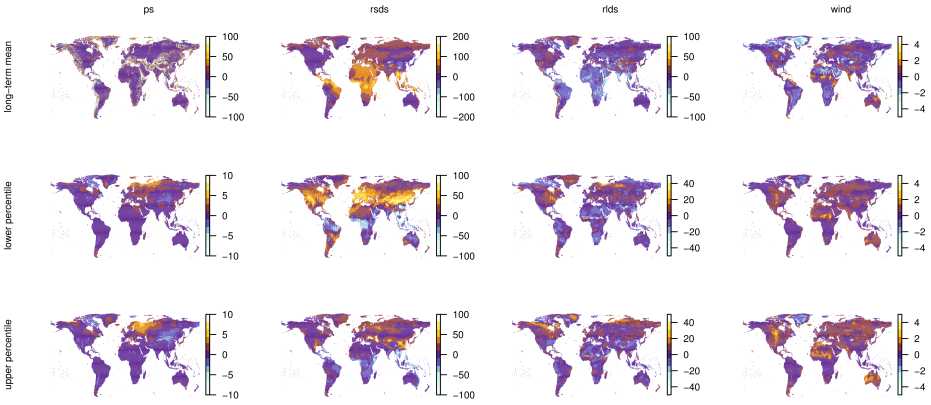

Figure S7: Differences between observations and the simulated surface pressure (ps in hPa), short wave downward radiation (rsds in W m^{-2}), long wave downward radiation (rlds in W m^{-2}) and wind speed (wind in m s^{-1}) in terms of the long-term mean and the lower and upper interpercentile ranges. Simulated values are interpolated to the resolution of the observational data set.